Available online at www.sciencedirect.com
SCIENCE DIRECT
Journal of Colloid and Interface Science 278 (2004) 497–507
JOURNAL OF Colloid and Interface Science
www.elsevier.com/locate/jcis

Transient electroosmotic flow induced by DC or AC electric fields in a curved microtube

W.-J. Luo *

Department of Electric Engineering, Far East College, Tainan, Taiwan

Received 2 February 2004; accepted 2 June 2004
Available online 17 July 2004

Abstract

This study investigates transient electroosmotic flow in a rectangular curved microtube in which the fluid is driven by the application of an external DC or AC electric field. The resultant flow-field evolutions within the microtube are simulated using the backwards-Euler time-stepping numerical method to clarify the relationship between the changes in the axial-flow velocity and the intensity of the applied electric field. When the electric field is initially applied or varies, the fluid within the double layer responds virtually immediately, and the axial velocity within the double layer tends to follow the varying intensity of the applied electric field. The greatest net charge density exists at the corners of the microtube as a result of the overlapping electrical double layers of the two walls. It results in local maximum or minimum axial velocities in the corners during increasing or decreasing applied electric field intensity in either the positive or negative direction. As the fluid within the double layer starts to move, the bulk fluid is gradually dragged into motion through the diffusion of momentum from the double layer. A finite time is required for the full momentum of the double layer to diffuse to the bulk fluid; hence, a certain phase shift between the applied electric field and the flow response is inevitable. The patterns of the axial velocity contours during the transient evolution are investigated in this study. It is found that these patterns are determined by the efficiency of momentum diffusion from the double layer to the central region of the microtube.

Keywords: Transient; Electroosmotic flow; DC or AC electric field; Momentum diffusion

1. Introduction

The term “electroosmotic flow” refers to fluid flow induced by an externally applied electric field along a charged surface. Electroosmotic flow is a fundamental electrokinetic phenomenon and has found a wide variety of practical applications. The recent rapid development of microfluidic systems designed for biological and chemical “laboratories on a chip” has prompted the search for dramatic improvements in the efficiency and throughput of these systems. It is often necessary to drive fluids from one part of a device to another, to control the fluid motion, to enhance mixing, or to separate fluids. Electroosmosis provides an attractive means of manipulating liquids in microdevices. One advantage of using this electrokinetic phenomenon is that the voltages applied at the device reservoirs can both control the bulk fluidic transport and cause the separation of the different components of a sample due to their differing electrophoretic mobility.

The mathematical model of electroosmotic flow in an ultrafine slit was formulated by Burgreen and Nakache [1] in 1964. Recently, Arulanandam and Li [2] presented a two-dimensional mathematical model for electroosmotic flow in a rectangular microchannel. Patankar and Hu [3] and Yang et al. [4] used numerical methods to simulate electroosmotic flow at the intersection of a cross-microchannel during a chemical-sample injection procedure. Bianchi et al. [5] applied the finite element method to simulate electroosmotic flow at a microscale T-junction. They showed that the velocity distribution of flow at the intersection is affected by the relative zeta potentials and channel widths. Mitchell et al. [6] developed meshless analysis based on the finite cloud method to simulate electroosmotic flow on various geometries. Their results indicated that the linear approximation of the Poisson–Boltzmann equation for large zeta

* Fax: +886-6-597-7570.
E-mail address: wjluo@cfd.es.ncku.edu.tw.

0021-9797/$ – see front matter
doi:10.1016/j.jcis.2004.06.017

potential still can predict the plug velocity accurately. Yang et al. [7] used numerical methods to concern the entrance effect in the microchannel by solving additional Nernst–Planck equations for ionic concentration.

Time-periodic electroosmotic flows and alternating-current electroosmosis have attracted considerable academic attention. Investigation of transient phenomena of electroosmotic flow is important for biochip operation and separation efficiency. Soderman and Jonsson [8] and Santiago [9] have presented a theoretical framework describing the behavior of the transient electroosmotic flow under the Debye–Hückel linear approximation. Oddy et al. [10] presented an analytic flow-field model for an axially applied AC electric field in an infinitely wide microchannel and demonstrated experimentally a series of schemes for enhanced species mixing in microfluidic devices. Dutta and Beskok [11] developed an analytic model for an applied sinusoidal electric field using a nonlinear Poisson–Boltzmann double-layer distribution. Studer et al. [12] established a fabrication technique which allowed the realization of microfluidic devices incorporating electrodes with smaller feature sizes and demonstrated that the resulting devices were capable of supporting such novel functionalities as the injection, mixing, and separation of biomolecules by means of AC electrokinetic pumping. Green et al. [13] applied a nonuniform AC electric field to an electrolyte using coplanar microelectrodes to generate steady fluid flow. The flow was driven at the surface of the electrodes so that it moved in a plane normal to the electrode surface. The impedance of the double layer on the electrodes and the potential drop across the double layer have been studied experimentally and theoretically using linear analysis. Erickson and Li [14] developed an analytical solution, via a Green's function formulation, for AC electroosmotic flow through a rectangular microchannel for the case of a sinusoidal applied electric field. Their results indicated that the steady time-periodic velocity profile is characterized by the ratio of the period of oscillation to the time scale for viscous diffusion, by the surface zeta-potential distribution, and by the channel aspect ratio.

The geometry of a microfluidic device is commonly characterized by a rectangular curved microtube. The flow-field conditions within such a microtube have a significant influence upon the performance of the device when it conducts the separation, extraction, and mixture of chemical or biological components. The present study applies a numerical approach to investigate time-periodic electroosmotic flow in a rectangular curved microtube. The investigations of transient behavior provide detailed insight into the characteristics of electroosmotic flow and are consequently of great importance in understanding and enhancing biochip operation. A numerical method is adopted in which the transient phenomena of electroosmotic flow are simulated using the Debye–Hückel linear approximation. Through the application of the backwards-Euler time-stepping method, a numerical solution is obtained for the stream-function and vorticity-transport equations, which govern the velocity fields of the electroosmotic flow. The transient behavior of the impulsively generated electroosmotic flow is then discussed in terms of the influence of the applied DC or AC electric field.

2. Governing equations and boundary conditions

This study considers a rectangular curved microtube with the same height and width of 30 μm. The tube is filled with an incompressible Newtonian electrolyte of uniform dielectric constant ε and viscosity μ. It is assumed that this fluid is in a stationary state initially. A fully developed flow field is then established in which the flow is driven by an applied DC or AC electric field. Since the characteristic length of the microtube is on the order of magnitude of 10 μm, the interaction of the fluid and the wall is significant and must therefore be considered in the theoretical model. A review of the related literature reveals that a theoretical model of the microchannel has been widely applied in previous studies. This model is described by the following set of equations: the Poisson–Boltzmann equation, the Laplace equation, and the Navier–Stokes equation, which comprises the body force terms from the Guoy–Chapman model. In applying this model, it is convenient to transform the toroidal coordinate system (R, Y, θ) to the related coordinate system (X, Y, Z), where $X = R - C$, $\mathrm{d}Z = C\,\mathrm{d}\theta$, and C is the radius of curvature, as shown in Fig. 1.

2.1. Double-layer field

When the liquid in the tube comes into contact with the solid wall, an interfacial charge is established. This charge causes the free ions in the liquid to rearrange to form a thin region with nonzero net charge density. This region is commonly referred to as the electrical double layer (EDL). According to electrostatic theory, the electrical potential distribution in the EDL region is governed by the Poisson–Boltzmann equation [15], which is expressed as

$$\frac{1}{(x+c)}\frac{\partial}{\partial x}\left[(x+c)\frac{\partial \psi}{\partial x}\right] + \frac{\partial^2 \psi}{\partial y^2} = \frac{2n_0 ze}{\varepsilon}\sinh(ze\psi/k_\mathrm{b}T),$$

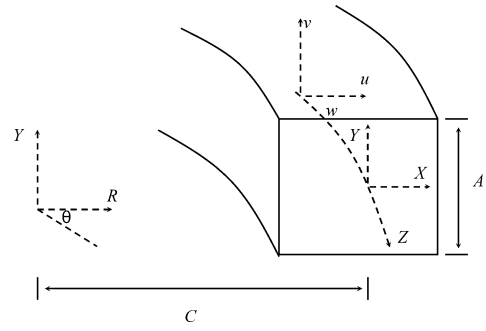

Fig. 1. Geometry of curved microtube and associated coordinate system. The directions of velocity (u, v, w) are defined in the figure.

where ε is the dielectric constant of the fluid medium, z is the valence, e is the charge of an electron, n_0 is the bulk electrolyte concentration, k_b is the Boltzmann constant, and T is the temperature. Nondimensional quantities (denoted by asterisks) can be defined as

$$x^* = \frac{x}{A}, \qquad y^* = \frac{y}{A}, \qquad \psi^* = \frac{ze\psi}{k_b T}.$$

The dimensionless nonlinear Poisson–Boltzmann distribution equation is then given by

$$\frac{1}{(x+\beta)}\frac{\partial}{\partial x}\left[(x+\beta)\frac{\partial \psi}{\partial x}\right] + \frac{\partial^2 \psi}{\partial y^2} = \kappa^2 \sinh(\psi), \tag{1}$$

where ψ is the nondimensional double-layer potential, $\kappa = A \times K$ is the nondimensional double-layer thickness, $K = (2n_0 z^2 e^2/\varepsilon\varepsilon_0 k_b T)^{1/2}$ is the Debye–Hückel parameter, A is the height of the rectangular cross section of the tube, and curvature ratio $\beta = C/A$. (Note that the asterisks are deliberately omitted in these equations.)

2.2. Electroosmotic flow field

When an external electric field is applied, the liquid flow induced by electroosmosis is governed by the general incompressible Navier–Stokes equation [11,16],

$$\rho\frac{\partial V}{\partial t} + \rho(V\cdot\nabla)V = -\nabla P + F + \mu\nabla^2 V. \tag{2}$$

If the gravity effect is neglected, the body force, F, occurs only as a result of the action of the applied electric field on the free ions within the EDL. This body force induces a bulk fluid motion generally referred to as electroosmotic flow.

The following nondimensional quantities (denoted by asterisks) can be introduced: nondimensional velocity: $u^* = u/(\upsilon/A)$ or $v^* = v/(\upsilon/A)$, nondimensional time: $t^* = t/(A^2/\upsilon)$, nondimensional pressure: $p^* = (p - p_{\text{ref}})/(\rho\upsilon^2/A^2)$, and nondimensional frequency: $\Lambda^* = A^2\Lambda/\upsilon$, where υ is the kinetic viscosity of the electrolyte, t is time, and Λ is the frequency of the applied electric field; i.e., $\Lambda = 2\pi f$. Hence, the continuity equation and Navier–Stokes equation of Eq. (2) can be rewritten as

$$\frac{1}{(x+\beta)}\frac{\partial}{\partial x}\big[(x+\beta)u\big] + \frac{\partial v}{\partial y} = 0, \tag{3a}$$

$$\frac{\partial u}{\partial t} + u\frac{\partial u}{\partial x} + v\frac{\partial u}{\partial y} - \frac{w^2}{(x+\beta)} + \frac{u}{(x+\beta)^2} + \frac{\partial p}{\partial x} - \frac{1}{(x+\beta)}\frac{\partial}{\partial x}\left[(x+\beta)\frac{\partial u}{\partial x}\right] - \frac{\partial^2 u}{\partial y^2} - G_x \sinh\psi\left(\frac{\partial \psi}{\partial x}\right) = 0, \tag{3b}$$

$$\frac{\partial v}{\partial t} + u\frac{\partial v}{\partial x} + v\frac{\partial v}{\partial y} + \frac{\partial p}{\partial y} - \frac{1}{(x+\beta)}\frac{\partial}{\partial x}\left[(x+\beta)\frac{\partial v}{\partial x}\right] - \frac{\partial^2 v}{\partial y^2} - G_x \sinh\psi\left(\frac{\partial \psi}{\partial y}\right) = 0, \tag{3c}$$

$$\frac{\partial w}{\partial t} + u\frac{\partial w}{\partial x} + v\frac{\partial w}{\partial y} + \frac{uw}{(x+\beta)} + \frac{w}{(x+\beta)^2} + \frac{\beta}{(x+\beta)}\frac{\partial p}{\partial z} - \frac{1}{(x+\beta)}\frac{\partial}{\partial x}\left[(x+\beta)\frac{\partial w}{\partial x}\right] - \frac{\partial^2 w}{\partial y^2} - G_x \sinh\psi\left(\frac{\beta}{(x+\beta)}\frac{\partial \phi}{\partial z}\right) = 0, \tag{3d}$$

where $G_x = 2n_0 k_b T/(\rho\upsilon^2/A^2)$ and ϕ is electrical potential. The magnitude of the axial pressure gradient is very small in comparison with that of the body force in a microtube. Hence, the axial pressure gradient can be neglected in Eq. (3d).

The stream function, S, is defined as

$$u = \frac{\beta}{(x+\beta)}\frac{\partial S}{\partial y}, \qquad v = -\frac{\beta}{(x+\beta)}\frac{\partial S}{\partial x}. \tag{4}$$

The continuity equation can then be satisfied by substituting Eq. (4) into Eq. (3a). The pressure and body force terms, P and F, can be eliminated from Eqs. (3b) and (3c) by cross-differentiation, i.e., by taking the curl of the two-dimensional momentum equation. The vorticity-transport equation can be derived as

$$(x+\beta)\frac{\partial \Omega}{\partial t} - \beta\frac{\partial S}{\partial y}\frac{\partial \Omega}{\partial x} - \beta\frac{\partial S}{\partial x}\frac{\partial \Omega}{\partial y} + 2w\frac{(x+\beta)}{\beta}\frac{\partial w}{\partial y} - \Omega\frac{2\beta}{(x+\beta)}\frac{\partial S}{\partial y} - \left[\frac{\partial}{\partial x}(x+\beta)\frac{\partial \Omega}{\partial x} + (x+\beta)\frac{\partial^2 \Omega}{\partial^2 y}\right] = 0. \tag{5}$$

Furthermore, the vorticity, Ω, is given by

$$\Omega + \frac{1}{(x+\beta)}\frac{\partial}{\partial x}\left[(x+\beta)\frac{\partial S}{\partial x}\right] + \frac{\partial^2 S}{\partial^2 y} - \frac{\beta}{(x+\beta)}\frac{\partial S}{\partial x} = 0. \tag{6}$$

For pure electroosmotic flow, the magnitude of the axial pressure gradient, $\partial p/\partial z$, is very small in comparison with that of the body force, F, in a microtube. Hence, the axial pressure gradient, $\partial p/\partial z$, in Eq. (3d) can be neglected in the case of fully developed flow. The zeta potential distribution in the EDL can be obtained by solving Eq. (1). Substitution of the calculated electric potential into Eq. (3d) yields the transient electroosmotic flow under an applied electric field by solving the simplified equation set of Eqs. (3d), (5), and (6). By taking the cross-differentiation operation, the total number of dependent variables is reduced to just three, (S, Ω, w), and the body force terms from the Guoy–Chapman model in Eqs. (3b) and (3c) can be discarded. The boundary conditions of zeta potential at four walls are −75 mV, and its corresponding dimensionless value is $\psi = -3$. Hence, the boundary conditions at the four walls of the microtube are given as follows.

(1) At left and right walls:

$$S = 0, \qquad \Omega + \frac{\partial^2 S}{\partial^2 x} = 0, \qquad w = 0, \qquad \psi = -3.$$

(2) At upper and lower walls:

$$S = 0, \qquad \Omega + \frac{\partial^2 S}{\partial^2 y} = 0, \qquad w = 0, \qquad \psi = -3.$$

3. Numerical method

The present numerical method employs the backwards-Euler time-stepping method to identify the evolutions of a flow driven by an applied DC or AC electric field. The computational domain is discretized into 121×121 nonequally-spaced grid points in both X- and Y-directions. The calculated solutions have been carefully proved to be independent of computational grid points and time step. The governing equations presented in Eqs. (3d), (5), and (6) are discretized by central differences of a second order to form a system of nonlinear algebraic equations,

$$H(S, \Delta t) = 0, \tag{7}$$

where S is the solution vector and Δt is the dimensionless marching time step.

The solution vector for various time-levels can be obtained via a sequence of iterations, $[S^{(\upsilon)}(t)]$, which is defined by

$$S^{(0)}(0) \equiv \text{initial state}, \tag{8a}$$

$$H_S\big(S^{(\upsilon)}, \Delta t\big)\big[S^{(\upsilon+1)}(t + \Delta t) - S^{(\upsilon)}(t + \Delta t)\big] = -H\big(S^{(\upsilon)}, \Delta t\big), \quad \text{where } \upsilon = 0, 1, 2, \ldots. \tag{8b}$$

In Eq. (8b), H_S is the Jacobian matrix of Eq. (7), and t is the nondimensional time.

A convergence criterion of $[S^{(\upsilon+1)}(t + \Delta t) - S^{(\upsilon)}(t + \Delta t)]^2/S(t)^2 < 10^{-16}$ is used to identify the convergence of the iteration process. Whether or not the iteration actually converges and, if it does, its convergence efficiency, are both determined by the accuracy of the initial estimate. An appropriate initial estimate ensures that the iteration will converge efficiently. An effective method of obtaining good initial estimates is to employ a Taylor expansion of a calculated convergent solution with respect to the parameter Δt,

$$S^{(0)}(t + \Delta t) = S(t) + \Delta t S_t(t). \tag{9}$$

Equation (7) is used to obtain S_t, which satisfies

$$H_S(S, \Delta t)S_t = -H_{\Delta t}(S, \Delta t). \tag{10}$$

The method described in Eqs. (8), (9), and (10) is known as the backwards-Euler time-stepping method. Since this method employs second-order accuracy in time, it is necessary to provide two initial solutions at the beginning of the time-stepping calculation. One of these solutions can be obtained from the initial state, while the other is obtained using the same numerical method, but with a first-order finite difference in time. Before the iteration algorithm is executed to obtain the convergence solution of the next time level, the predictor step in Eqs. (9) and (10) is applied to generate accurate estimates of the solution. Hence, the calculation algorithm is extremely effective and generally converges quadratically. For the detailed algorithm of the numerical method please refer to Yang and Luo [17].

4. Results and discussion

4.1. Transient electroosmotic flow induced by DC electric field

The present study investigates transient electroosmotic flow in a curved microtube with a curvature ratio of $\beta = 50$, a length and width of 30 μm, and an aspect ratio of 1. The relevant parameters of the microtube are presented in Table 1. The microtube is filled initially with a stationary fluid, which is then driven through the microtube by the initial impulse

Table 1
Typical values of the relevant quantities

A	Height of the rectangular curved tube	30 μm
β	Curvature ratio	50
C	Radius of curvature	1.5 mm
μ	Viscosity of fluid	0.90×10^{-3} N s m^{-2}
ρ	Density of fluid	10^3 kg m^{-3}
ζ	Concentration of ions	10^{-6} M
ε	Dielectric constant	78.3
ε_0	Permittivity of vacuum	8.854×10^{-12} F m^{-1}
e	Charge of an electron	1.6021×10^{-19} c
z	Valence	1
n_0	Bulk electrolyte concentration	6.022×10^{20} m^{-3}
k_b	Boltzmann constant	1.38×10^{-23} J K^{-1}
T	Absolute temperature	298.16 K
ψ	Double-layer potential	−75 mV
Λ^*	Nondimensional frequency of the applied AC electric field	1

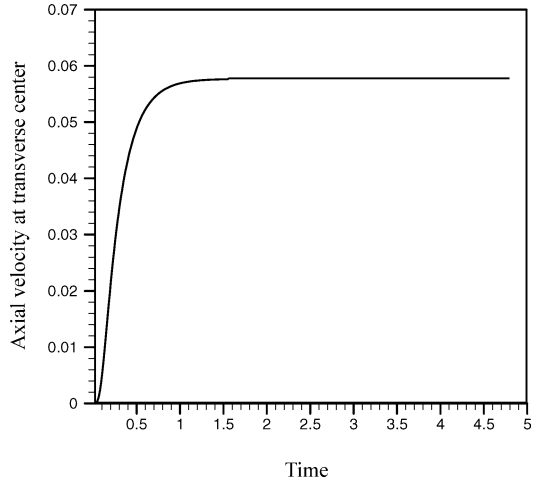

Fig. 2. Variation in axial velocity of flow at transverse center of microtube over time. Note that the flow is driven through the microtube under the influence of an initial impulse supplied by the applied DC electric field.

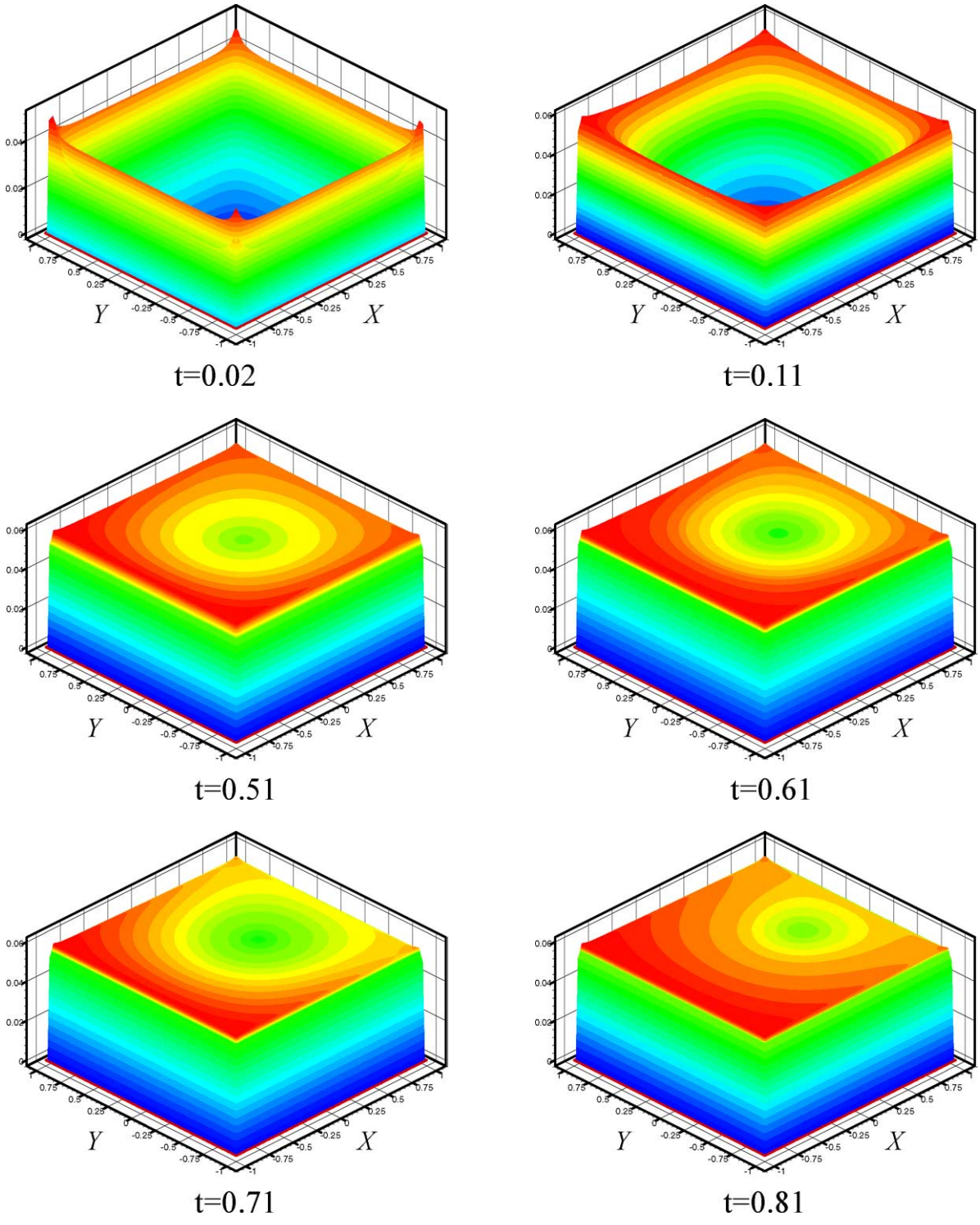

Fig. 3. Evolution of axial-velocity contours during period of transient response under influence of impulse supplied by applied DC electric field.

provided by the applied DC electric field. The dimensionless intensity of this electric field along the axial direction is $\partial\phi/\partial z = 52.49$. Fig. 2 presents the variation in the axial velocity of the flow at the transverse center of the microtube over time. When the electric field is initially applied, the fluid within the double layer responds virtually immediately, but the bulk fluid in the microtube remains stationary. However, as the fluid within the double layer starts to move, the bulk fluid is gradually dragged into motion through the diffusion of momentum from the double layer. A finite time is required for full momentum diffusion from the double layer to the bulk fluid, and hence the flow in the central region of the microtube evolves through a period of transient response before attaining a steady-state flow. Fig. 2 indicates

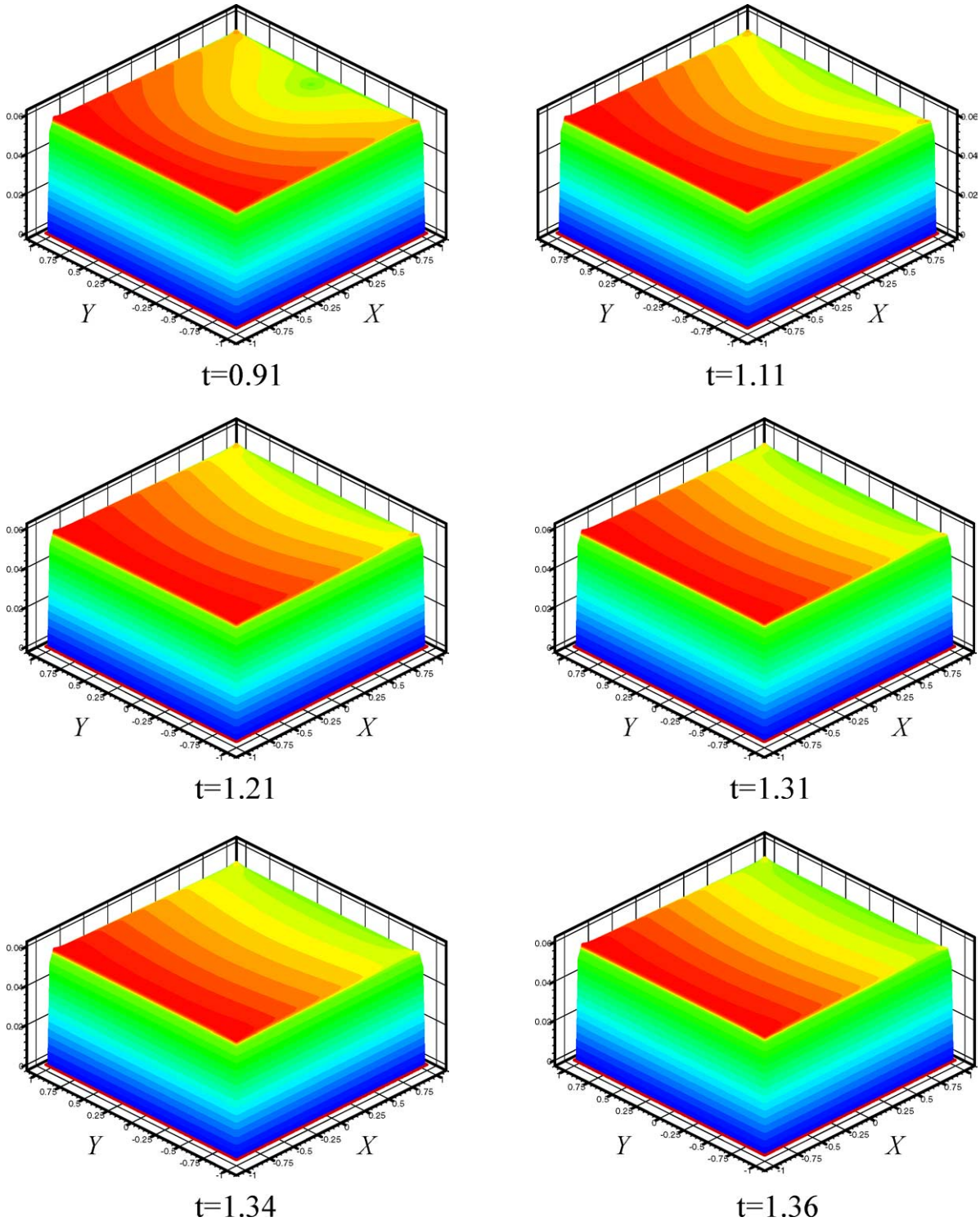

Fig. 3. (Continued).

that the dimensionless transient response time is approximately $t = 1.36$.

Fig. 3 illustrates the evolution of the axial velocity contours during the period of transient response. Initially, the impulse provided by the applied DC electric field drives the fluid within the double layer in the axial direction, and the axial velocity contours adopt a ringlike form. The intersection of two walls causes overlapping of the double layer, and hence a greater net charge density accumulates in each corner of the microtube. These net-charge-density peaks cause the particles in the corners to respond rapidly to the influence of the applied electric field. Hence, as time elapses, the fluid within the double layer rapidly accelerates in the axial direction. It is noted that the maximum velocity occurs at the

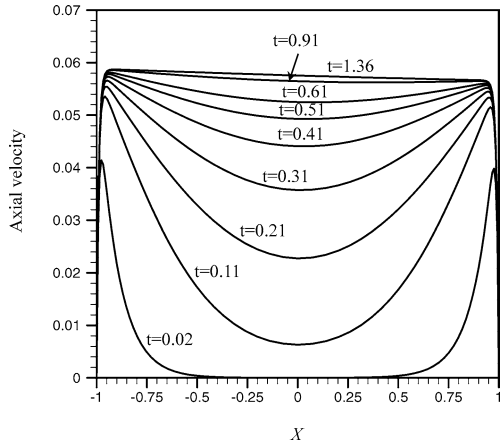

Fig. 4. Axial velocity distribution along X-coordinate during period of transient response from $t = 0$ to $t = 1.36$.

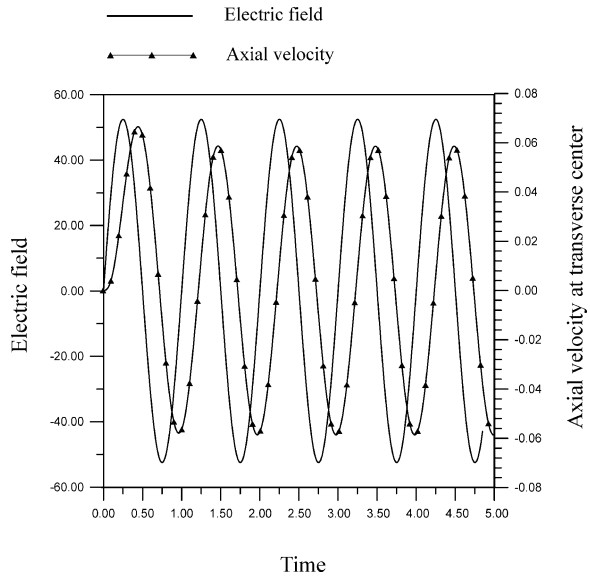

Fig. 5. Variations in applied AC electric field and axial velocity of electroosmotic flow in transverse center of microtube over time.

corners of the microtube. The momentum of the double layer gradually diffuses to the central region, and therefore the axial velocity contours assume a C-like form. As further time elapses, the contours with higher axial velocity gradually accumulate near the inner side. Under steady-state conditions, the axial-velocity contours demonstrate a stratified form.

Fig. 4 indicates the axial velocity distribution along the X-coordinate during the period of transient response from $t = 0$ to $t = 1.36$. During this period, the axial velocity in the transverse center of the microtube increases from zero to its maximum value. Under the influence of the initial impulse provided by the applied DC electric field, the fluid near the inner and outer walls accelerates rapidly in the positive axial direction. However, the bulk fluid is only gradually dragged into motion in the positive direction by the diffusion of momentum from the double layer. At $t = 1.36$, the axial velocity in the transverse section is equal to approximately 0.057.

4.2. Transient electroosmotic flow induced by AC electric field

In this particular investigation, the fluid is driven through the microtube by an applied AC electric field. The dimensionless electric field within the microtube is given by $\partial\phi/\partial z = 52.49\sin(2\pi t)$. Fig. 5 presents the variations in the applied electric field along the axial direction and the axial velocity of the flow in the transverse center of the microtube over time. The amplitude and the cycle period of the applied AC electric field are 52.49 and 1, respectively. In general, it can be seen that the axial velocity tends to follow the varying intensity of the applied electric field; i.e., the flow accelerates as the intensity of the applied electric field increases and decelerates as the intensity of the applied electric field decreases. However, it is noted that the variation in the flow velocity lags behind that of the electric field by a phase shift of approximately $(\pi/2)°$. When the electric field is initially applied, the fluid within the double layer starts to move, but the fluid in the central region of the microtube remains stationary. As described previously, a finite time is required for the momentum of the double layer to diffuse to the bulk fluid, and hence a certain degree of phase shift between the applied electric field and the flow response is inevitable. Finally, the central-region flow attains a steady-state condition, in which the change in velocity matches that of the applied electric field. It can be shown that the time for the velocity in the central region of the microtube to attain a steady-state condition is approximately 0.7 of the dimensionless transient response time.

Fig. 6 presents the evolution of the axial velocity contours in the transverse section during the period from $t = 1$ to $t = 1.5$. At $t = 1$, the intensity of the applied electric field is zero, and the flow in the center of the microtube moves at its maximum velocity in the negative direction. It can be seen that the preceding negative electric field intensity causes the axial velocity contours to adopt a ringlike form, in which the innermost contours indicate the highest axial velocity in the negative direction. As further time elapses, the fluid particles within the double layer are rapidly driven in the positive direction under the influence of the applied AC electric field. Since the peak net charge density occurs at the corners of the microtube, the maximum velocity of the flow also takes place at each corner. At $t = 1.1$, the flow velocity near the four walls continues to increase, and the resulting momentum diffusion causes the region of flow with a positive velocity to spread gradually from the double layer toward the central region of the microtube. Finally, at $t = 1.25$, the region of flow in the positive direction expands to the point where it occupies almost the entire microtube profile. Meanwhile, the velocity of the flow in the center of the tube decreases to zero, as shown in Fig. 6. As the elapsed time increases further, the intensity of the electric field gradually decreases, and hence the positive axial velocity of the flow within the double layer decreases. The peaks

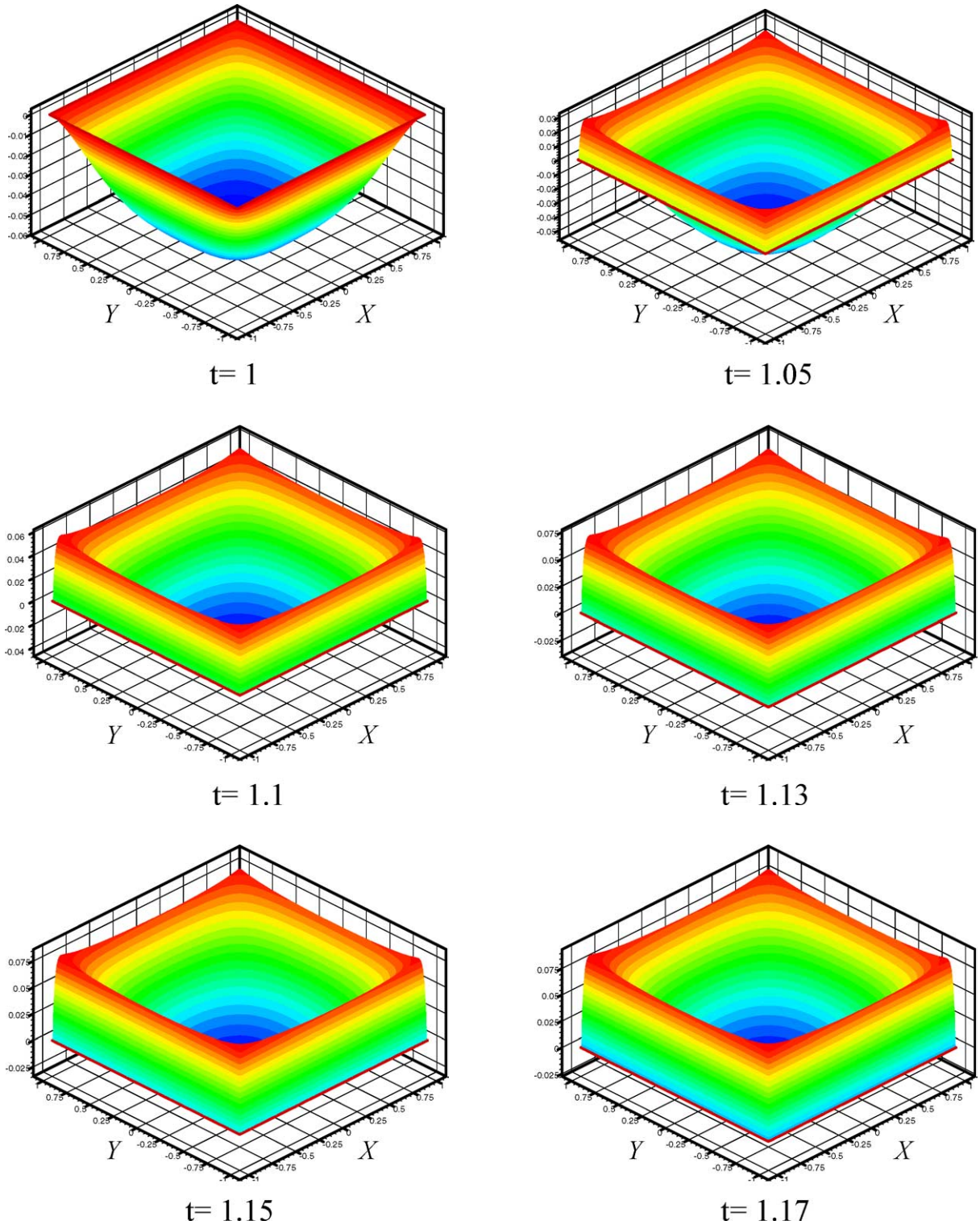

Fig. 6. Evolution of axial-velocity contours in transverse section during period from $t = 1$ to $t = 1.5$ under influence of applied AC electric field.

in the net charge density cause particles in the corners to respond rapidly to the change in the applied AC electric field, and consequently there is a reduction in the local maximum velocity at each corner. Meanwhile, inertia forces cause the axial velocity of the flow in the center of the microtube to continue to increase in the positive direction. At $t = 1.4$, the velocity of the bulk flow in the positive direction reaches an almost equal value, while the axial flow at the corners attains a local minimum value. At $t = 1.45$, the positive intensity of the applied AC electric field continues to decrease, and momentum diffusion causes the region of flow with slower positive axial velocity to expand toward the central region.

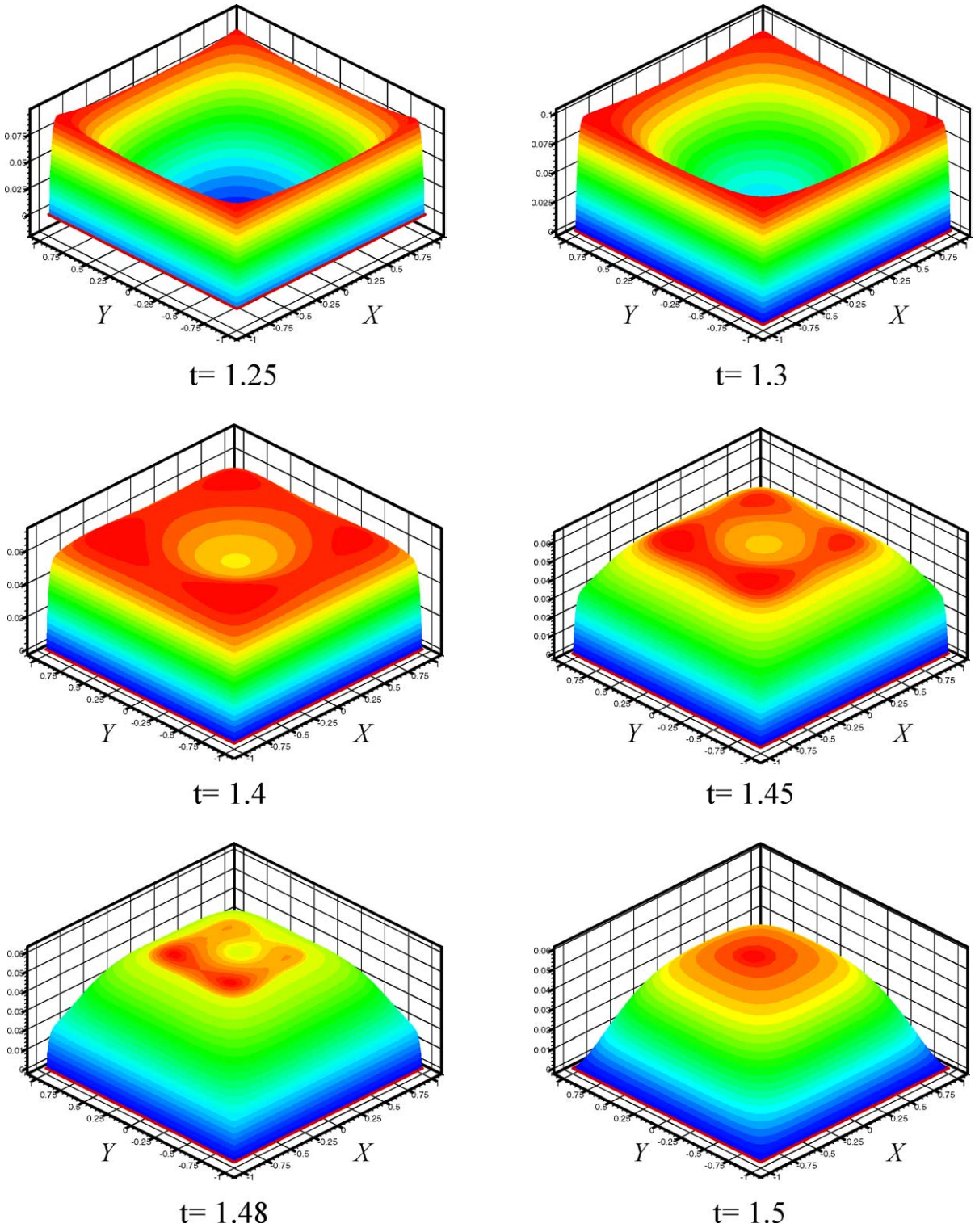

Fig. 6. (Continued).

At $t = 1.5$, the axial velocity in the central region attains its maximum value. At $t = 1.5$, it is noted that the axial-flow-velocity contours strongly resemble those evident at $t = 1$ in terms of their shape. However, it is important to note that the direction of the axial velocity is reversed. During the second half of the cycle, from $t = 1.5$ to $t = 2$, the variation of the applied AC electric field intensity is the mirror image of the variation described from $t = 1$ to $t = 1.5$, and accordingly, the axial flow velocity in the central region of the microtube reverses from a positive direction to a negative direction. Essentially, the evolution of the axial velocity contours during the cycle from $t = 1.5$ to $t = 2$ follows the same process as

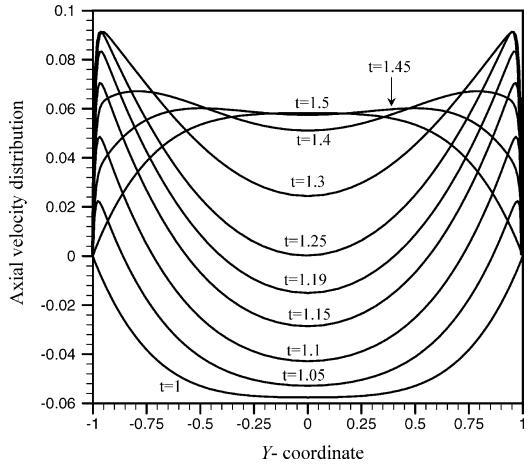

Fig. 7. Axial velocity distribution along Y-coordinate during period from $t = 1$ to $t = 1.5$.

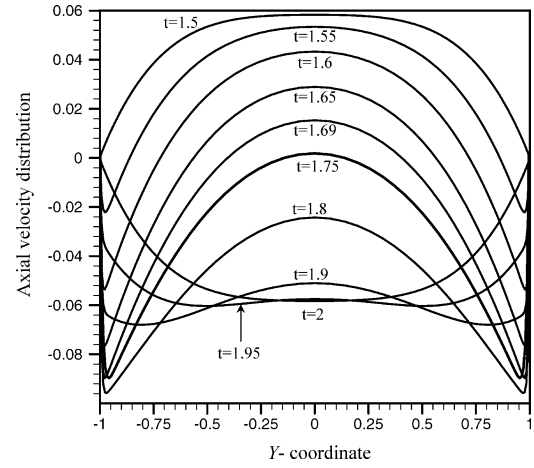

Fig. 9. Axial velocity distribution along Y-coordinate during period from $t = 1.5$ to $t = 2.0$.

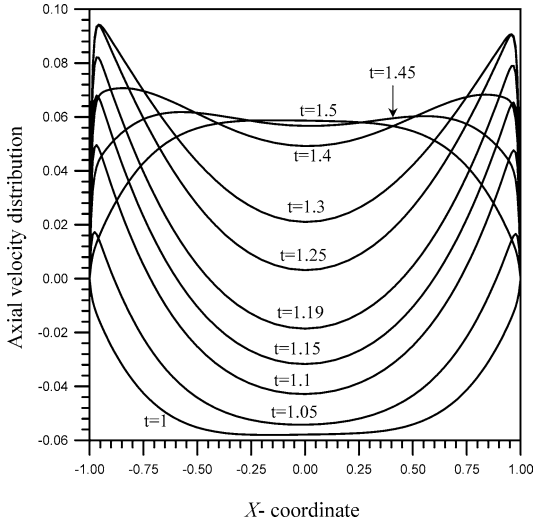

Fig. 8. Axial velocity distribution along X-coordinate during period from $t = 1$ to $t = 1.5$.

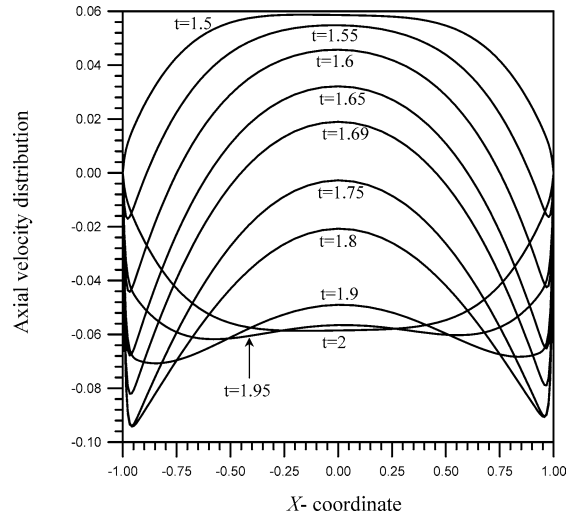

Fig. 10. Axial velocity distribution along X-coordinate during period from $t = 1.5$ to $t = 2.0$.

that described for $t = 1$ to $t = 1.5$. However, it is noted that the axial flow directions are reversed. Consequently, at $t = 2$, the axial velocity contours are identical to those observed at $t = 1$.

Figs. 7 and 8 indicate the axial velocity distribution along the Y-coordinate and X-coordinate during the period from $t = 1$ to $t = 1.5$. The axial velocity in the transverse center of the microtube gradually increases from its minimum value to its maximum value during this period. It is noted that the intensity of the applied AC electric field gradually increases from $t = 1$ to $t = 1.25$, and then decreases from $t = 1.25$ to $t = 1.5$. Consequently, the fluid near the upper and lower walls accelerates rapidly in the positive direction between $t = 1$ and $t = 1.25$, and then decelerates in the positive direction from $t = 1.25$ to $t = 1.5$. However, the movement of fluid within the double layer only gradually drags the bulk fluid into motion in the positive direction, since the momentum diffusion requires a finite time to take effect. Due to the centrifugal effect, the magnitude of axial velocity near the inner wall ($X = -1$) is greater than that near the outer wall ($X = 1$) at different instants, as shown in Fig. 8.

Figs. 9 and 10 indicate the axial velocity distribution along the Y-coordinate and X-coordinate during the period from $t = 1.5$ to $t = 2$. During this period, the axial velocity in the transverse center of the microtube gradually decreases from its maximum value to its minimum value. The intensity of the applied AC electric field gradually increases between $t = 1.5$ and $t = 1.75$ and then decreases from $t = 1.75$ to $t = 2.0$ in the negative direction. Consequently, the fluid near the upper and lower walls accelerates rapidly in the negative direction from $t = 1$ to $t = 1.75$ and then decelerates in the negative direction from $t = 1.75$ to $t = 2.0$. However, the bulk fluid is only gradually dragged into motion in the negative direction due to the delay associated with the momentum diffusion from the double layer. Due to the centrifugal effect, the magnitude of axial velocity near the inner wall ($X = -1$) is greater than that near the outer wall ($X = 1$) at different instants, as shown in Fig. 10.

5. Summary

The flow-field conditions within the electrokinetic microchannel of a microfluidic device have a significant influence upon the performance of the device in the separation, extraction, and mixing of chemical or biological components. Therefore, it is essential to develop a thorough understanding of the evolution of these flow-field conditions when such a device is designed. The present study has considered the case of transient electroosmotic flow in a rectangular curved microtube in which the fluid is driven by an external DC or AC electric field. The resultant flow-field evolutions within the microtube have been investigated using the backwards-Euler time-stepping numerical method to clarify the relationship between changes in the intensity of the applied electric field and the distribution of the fluid flow in the axial direction.

For the case of transient electroosmotic flow with an external DC electric field, initially, the impulse provided by the applied DC electric field drives the fluid within the double layer in the axial direction, and the axial-velocity contours adopt a ringlike form. The greater net charge density in the corners causes the particles in the corners to respond rapidly to the influence of the applied electric field, and the maximum velocity occurs at the corners of the microtube. The momentum of the double layer gradually diffuses to the central region, and therefore the axial-velocity contours assume a C-like form. As further time elapses, the contours with higher axial velocity gradually accumulate near the inner side. Under steady-state conditions, the axial-velocity contours demonstrate a stratified form.

This study has also considered the application of a sinusoidal electric field to the flow in the curved microtube and has investigated the relationship between the periodic electric field and the corresponding evolution of the axial-flow velocity. The results indicate that the flow in the center of the microtube initially exhibits a transient response when the electric field is applied and then attains a steady-state condition. The greater net charge density in the corners of the microtube results in local maximum or minimum axial velocities in the corners during increasing or decreasing applied electric field intensity in either the positive or negative direction. It has been shown that the axial-flow velocity tends to follow the varying intensity of the applied AC electric field. When the electric field is initially applied, a certain phase shift between the applied electric field and the flow response is inevitable because a finite time is required for the momentum of the double layer to diffuse to the bulk fluid. The evolution process of the axial velocity contours during a half cycle follows the same process as for the preceding half cycle. However, the axial flow directions are reversed.

Acknowledgment

The author acknowledges financial support for this study provided by the National Science Council under Grant NSC 91-2212-E-269-010.

References

[1] D. Burgreen, F.R. Nakache, J. Phys. Chem. 68 (1964) 1084.
[2] S. Arulanandam, D. Li, Colloids Surf. A 161 (2002) 89.
[3] N.A. Patankar, H.H. Hu, Anal. Chem. 70 (1998) 1870.
[4] R.-J. Yang, L.-M. Fu, Y.-C. Lin, J. Colloid Interface Sci. 239 (2001) 98.
[5] F. Bianchi, R. Ferrigno, H.H. Girault, Anal. Chem. 72 (2000) 1987.
[6] M.J. Mitchell, R. Qiao, N.R. Aluru, J. Microelectromech. Syst. 9 (2000) 4.
[7] R.-J. Yang, L.-M. Fu, C.-C. Hwang, J. Colloid Interface Sci. 244 (2001) 173.
[8] O. Soderman, B. Jonsson, J. Chem. Phys. 105 (1996) 10300.
[9] J.G. Santiago, Anal. Chem. 73 (2001) 2353.
[10] M.H. Oddy, J.G. Santiago, J.C. Mikkelsen, Anal. Chem. 73 (2001) 5822.
[11] P. Dutta, A. Beskok, Anal. Chem. 73 (2001) 5097.
[12] V. Studer, A. Pepin, Y. Chen, A. Ajdari, Microelectron. Eng. 61–62 (2002) 915.
[13] N.G. Green, A. Ramos, A. Gonzalez, H. Morgan, A. Castellanos, Phys. Rev. E 61 (2000) 4011.
[14] D. Erickson, D. Li, Langmuir 19 (2003) 5421.
[15] R.J. Hunter, Zeta Potential in Colloid Science: Principals and Applications, Academic Press, New York, 1981.
[16] C. Yang, D. Li, Colloids Surf. A 143 (1998) 339.
[17] R.-J. Yang, W.-J. Luo, Theor. Comput. Fluid Dynam. 16 (2002) 115–131.